

PLUTINO DETECTION BIASES, INCLUDING THE KOZAI RESONANCE

S. M. LAWLER¹, B. GLADMAN¹
Draft version October 18, 2018

ABSTRACT

Because of their relative proximity within the transneptunian region, the plutinos (objects in the 3:2 mean-motion resonance with Neptune) are numerous in flux-limited catalogs, and well-studied theoretically. We perform detailed modelling of the on-sky detection biases for plutinos, with special attention to those that are simultaneously in the Kozai resonance. In addition to the normal 3:2 resonant argument libration, Kozai plutinos also show periodic oscillations in eccentricity and inclination, coupled to the argument of perihelion (ω) oscillation. Due to the mean-motion resonance, plutinos avoid coming to pericenter near Neptune’s current position in the ecliptic plane. Because Kozai plutinos are restricted to certain values of ω , perihelion always occurs out of the ecliptic plane, biasing ecliptic surveys against finding these objects. The observed Kozai plutino fraction $f_{\text{koz}}^{\text{obs}}$ has been measured by several surveys, finding values between 8% and 25%, while the true Kozai plutino fraction $f_{\text{koz}}^{\text{true}}$ has been predicted to be between 10% and 30% by different giant planet migration simulations. We show that $f_{\text{koz}}^{\text{obs}}$ varies widely depending on the ecliptic latitude and longitude of the survey, so debiasing to find the true ratio is complex. Even a survey that covers most or all of the sky will detect an apparent Kozai fraction that is different from $f_{\text{koz}}^{\text{true}}$. We present a map of the on-sky plutino Kozai fraction that would be detected by all-sky flux-limited surveys. This will be especially important for the Panoramic Survey Telescope & Rapid Response System (Pan-STARRS) and Large Synoptic Survey Telescope (LSST) projects, which may detect large numbers of plutinos as they sweep the sky. $f_{\text{koz}}^{\text{true}}$ and the distribution of the orbital elements of Kozai plutinos may be a diagnostic of giant planet migration; future migration simulations should provide details on their resonant Kozai populations.

1. INTRODUCTION

Plutinos are trans-Neptunian objects (TNOs) that are in the 3:2 mean-motion resonance with Neptune, meaning that in the time it takes Neptune to complete three orbits of the Sun, plutinos complete two orbits. Plutinos are named after Pluto, which was the first known resonant TNO, discovered to be so by examination of a numerical orbital integration (Cohen and Hubbard 1964). This same technique is currently used to confirm the resonant nature of plutinos (and other resonant TNOs; Gladman et al. 2008; Lykawka and Mukai 2007). Several of the first TNOs that were discovered in the early 1990s were also found to be plutinos (Davies et al. 2008). Plutinos are among the easier TNOs to observe; their semimajor axis of approximately 39.5 AU places them near the inner edge of the Kuiper Belt. Discovery is also helped by the high eccentricities many plutinos possess, causing close-in pericenters and lower apparent magnitudes, and thus brighter objects (this is an extremely strong effect since the TNOs are observed with reflected light, so their flux is proportional to distance⁻⁴). Plutinos (and other resonant TNOs) can have lower perihelia than non-resonant TNOs because the mean-motion resonance protects them from close encounters with Neptune (e.g. Malhotra 1996).

As of November 2012 there were 244 plutinos listed in the Minor Planet Center (MPC) database. However, only about 120 of these have high-quality multiopposition orbits, allowing numerical orbital integra-

tions (Lykawka and Mukai 2007; Gladman et al. 2008) to prove that the objects are truly resonant (showing libration of the resonant angle; see Section 2), and not just located near the resonance phase space.

This paper will highlight the special selection effects caused by the Kozai resonance within the 3:2 resonance. “Kozai plutinos” are TNOs that are simultaneously in the 3:2 mean-motion resonance with Neptune and in the Kozai resonance. Pluto was the first known Kozai resonator (Williams and Benson 1971).

What is now known as the Kozai resonance was first described for high-inclination asteroids by Kozai (1962). This effect occurs when a small body in orbit around a large central mass is perturbed by a third mass at high relative orbital inclination i . In the case of the trans-Neptunian region, the small bodies are the TNOs themselves, and the high relative inclination perturber is Neptune, and to a smaller degree the other planets. Any gravitational perturbations on the orbit of a small body cause ω to change. Most of the time, this causes ω to precess, but under the special conditions that the perturber is at high relative inclination, ω will oscillate instead: this is the signature of the Kozai resonance. When ‘near’ the resonance in phase space, the ω evolution becomes highly non-uniform (sometimes called the Kozai effect rather than resonance). In either case, one observes coupled e and i oscillations correlated with the value of ω . For non-resonant TNOs, Thomas and Morbidelli (1996) show that the Kozai resonance only occurs at extremely large eccentricity. However, inside mean-motion resonances, the Kozai resonance can appear at moderate i (e.g. Gallardo et al. 2012). This is how Pluto can show

¹Department of Physics and Astronomy, 6224 Agricultural Road, University of British Columbia, Vancouver, BC V6T 1Z1

Kozai oscillations despite being at the relatively low inclination of 17° .

Lykawka and Mukai (2007) presented the largest collection of plutinos that has been analyzed for Kozai resonance, after combing the contents of the Minor Planet Center (MPC) database at the time. They found that 22 out of 100 plutinos were solidly in the Kozai resonance, with ω oscillating around 90° or 270° , and in one case around 0° . Unfortunately, the MPC database’s collection of detections from many different non-uniform surveys does not allow for easy debiasing. Because of this, it is very difficult to measure the true fraction of Kozai versus non-Kozai plutinos from this dataset.

This manuscript was motivated by the results of the Canada-France Ecliptic Plane Survey (CFEPS; Jones et al. 2006; Kavelaars et al. 2009; Petit et al. 2011; Gladman et al. 2012), which detected and then re-acquired nearly 200 TNOs, including 24 plutinos, to produce high-quality orbits and orbital classifications. This survey was well calibrated: tracking efficiencies and magnitude depths are precisely known for each pointing. Because of this, the survey could be debiased to produce absolute populations. Two of the 24 detected Plutinos in the survey were found to be in the Kozai resonance upon examination of a 10 Myr orbital integration. Because 8% of the CFEPS-discovered plutinos were Kozai plutinos, in order to properly debias CFEPS’s result to produce the absolute population and orbital element distribution of the plutinos, this Kozai component had to be included and properly modelled (Gladman et al. 2012).

Though this paper only discusses plutinos in the Kozai resonance, Lykawka and Mukai (2007) also catalogued Kozai resonators in the 5:3, 7:4, and 2:1 mean-motion resonances. Other resonances can also exhibit Kozai oscillations in some portion of the resonant phase space.

This paper provides a basic understanding of the Kozai resonance within the 3:2, how the Kozai dynamics affect plutino observations, and introduces possible uses for this resonance in distinguishing between different giant planet migration models. Section 2 discusses in-depth the dynamical requirements for a TNO to be in a mean-motion resonance. Section 3 presents toy models of the 3:2 resonance (Sections 3.1 and 3.2), in order to demonstrate the effect of libration, and finally gives a realistic plutino distribution (Section 3.3). Section 4 discusses both the dynamics of the Kozai plutinos and the on-sky detection biases that result from the dynamical constraints placed on the Kozai plutinos. Section 5 gives a summary of how we simulate the plutino population. This simulation is used in Section 6 to show biases that observers will encounter on different parts of the sky in detecting Kozai and non-Kozai plutinos. Section 7 gives a discussion of previous observations of Kozai plutinos and of theoretical predictions in the literature. And finally, Section 8 discusses future observations that may help constrain the Kozai fraction and the distribution of the orbital elements of Kozai plutinos.

2. RESONANT DYNAMICS

Here we will discuss Plutino dynamics, and how resonant objects are identified in orbital integrations. Much of this discussion can be generalized to other mean-motion resonances. Figure 1 defines the usual heliocentric ecliptic orbital elements.

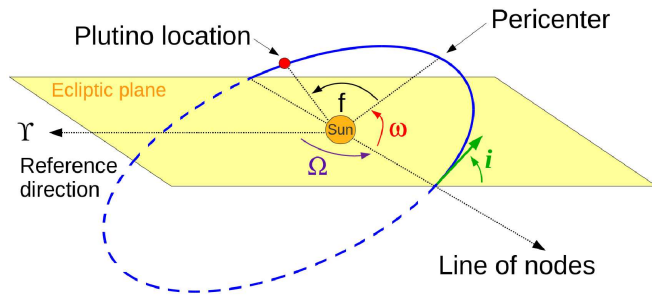


FIG. 1.— Ω is the longitude of the ascending node, ω is the argument of pericenter, and f is the true anomaly. The mean anomaly \mathcal{M} is the time since the last pericenter times the mean motion: $2\pi/P$. The mean longitude $\lambda = \Omega + \omega + \mathcal{M}$, and the longitude of pericenter $\varpi = \Omega + \omega$.

Resonances are diagnosed by inspecting the evolution of an object’s orbital elements during a numerical integration (Figure 2). The integration must be long enough that the Myr-timescale Kozai oscillations are visible. If the object inhabits the $j:k$ mean-motion resonance with Neptune, the primary resonant angle

$$\phi_{jk} = j\lambda - k\lambda_N - (j - k)\varpi \quad (1)$$

will be confined and will not take on all values 0° to 360° over the course of the integration. λ is the mean longitude of the object

$$\lambda = \Omega + \omega + \mathcal{M}, \quad (2)$$

which gives the angle to the position of the object relative to the reference direction. λ_N is the mean longitude of Neptune, giving the angle to Neptune’s position relative to the reference direction. $\varpi = \Omega + \omega$ is the longitude of pericenter, which is the broken angle locating the object’s pericenter relative to the reference direction. The amplitude of the ϕ_{jk} oscillation during the integration gives the libration amplitude A_{jk} of the object.

All plutinos by definition inhabit the 3:2 mean-motion resonance with Neptune, with a resonant argument

$$\phi_{32} = 3\lambda - 2\lambda_N - \varpi. \quad (3)$$

A feature of the Kozai resonance (discussed in detail in Section 4) is coupled oscillation in ω , eccentricity e , and inclination i (see Figure 2). e and i are anti-correlated, and ω oscillates around 90° or 270° (or temporarily around 0° or 180° ; Nesvorný and Roig 2000; Lykawka and Mukai 2007). Figure 2 shows a 10 Myr orbital integration of the Kozai plutino 28978 Ixion, showing the characteristic oscillations of e , i , and ω . For comparison, Figure 2 also shows a non-Kozai plutino and a non-resonant TNO nearby in semimajor axis.

3. NON-KOZAI PLUTINOS

To orient the reader and make several important points, we first discuss toy models and then a realistic libration amplitude distribution for the plutinos, ignoring the Kozai component until Section 4.

3.1. \mathcal{O}^p libration amplitude toy model

Due to the plutino resonance condition (Equation 3), the location where the Plutinos can come to pericenter is restricted. This is what allows resonant TNOs to remain stable on timescales of the age of the solar system,

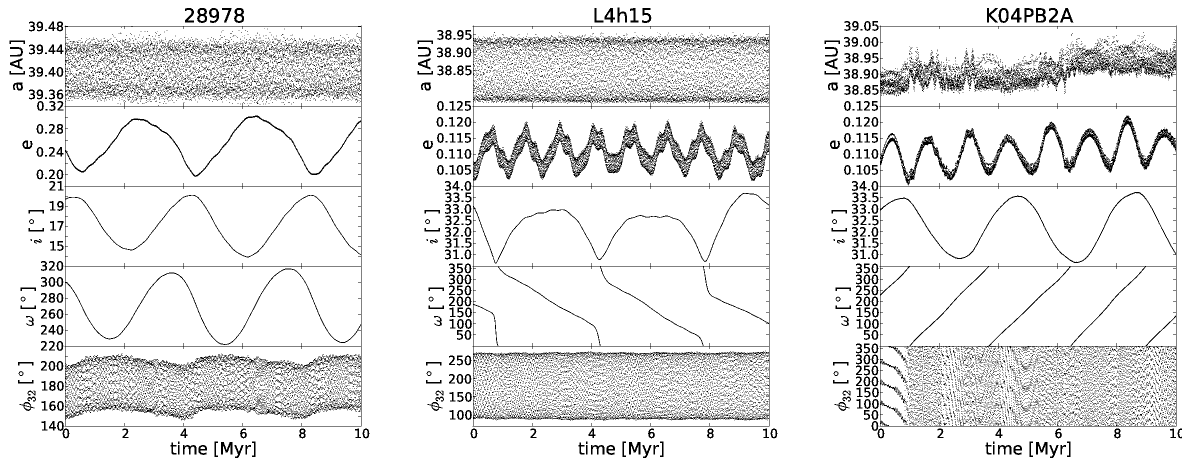


FIG. 2.— Barycentric orbital elements over the course of 10 Myr orbital integrations of the Kozai plutino 28978 Ixion (left), the CFEPS-discovered non-Kozai plutino L4h15 (2004 HB₇₉; center), and a non-resonant TNO (2004 PA₁₁₂; right) for comparison. In both resonant cases, the resonant argument ϕ_{32} librates around 180° (lower panels) because of the 3:2 mean-motion resonance with Neptune. The Kozai plutino 28978 Ixion’s integration also shows oscillations in ω around 270° with coupled, anti-correlated oscillations in e and i . The integrations of the non-Kozai plutino and non-resonant TNO both show oscillations in e and i , but they are not coupled, and ω circulates. Note that oscillations in semimajor axis and ϕ_{32} happen on much faster timescales (few thousand years) than the Kozai oscillations (few million years), and that the oscillations in semimajor axis are much larger for the resonant TNOs than the non-resonant one.

despite having orbits that in some cases cross the orbit of Neptune. The resonant angle ϕ_{32} librates around $180^\circ \pm 360^\circ \times k$, where k is an integer (using $\phi_{32} = 180^\circ$ or -180° is sufficient to include plutinos at all angles from Neptune). At pericenter, $\mathcal{M} = 0$, and at that moment equation 2 implies $\lambda = \Omega + \omega = \varpi$. For a plutino with libration amplitude $A_{32} = 0^\circ$, $\phi_{32} = 180^\circ$ always, and

$$\begin{aligned} 180^\circ &= 3\varpi - 2\lambda_N - \varpi \\ \varpi &= \lambda_N + 90^\circ \end{aligned} \quad (4)$$

So the plutino always comes to pericenter 90° away from Neptune’s position. This is shown in Figure 3. Because $\phi_{32} = -180^\circ$ is also valid, another perihelion occurs with $\varpi = \lambda_N - 90^\circ$. The two points on the sky where a $A_{32} = 0^\circ$ plutino comes to pericenter (in the ecliptic plane, at $\lambda_N \pm 90^\circ$), are very important in this paper, so to avoid confusion we will refer to these as the “orthoneptune points”.

3.2. 95° libration amplitude toy model

Real plutinos possess non-zero libration amplitudes; A_{32} for known plutinos with well-characterized orbits ranges between 20° and 130° (Lykawka and Mukai 2007; Gladman et al. 2012). These libration amplitudes lead to different selection effects: during each ϕ_{32} libration period the perihelion direction oscillates around the orthoneptune points roughly sinusoidally in time with amplitude $A_{32}/2$. Equation 3 shows that the maximum excursion from the orthoneptune points occurs when ϕ_{32} is at a maximum or minimum. This means that plutinos spend more time near the extrema allowed by their libration amplitudes, and are actually more likely to be detected there. We demonstrate this using a population of plutinos with $A_{32} = 95^\circ$ (see Figure 4 and caption). To avoid confusion, all the plutinos in this toy model have 0° inclination to the ecliptic, and all have the same eccentricity. $A_{32} = 95^\circ$ is chosen because it was found to be the most common plutino libration amplitude by CFEPS (Gladman et al. 2012).

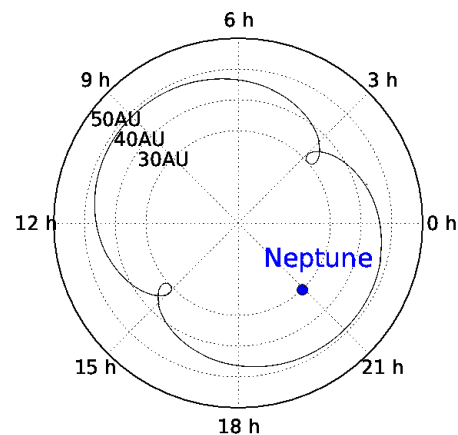


FIG. 3.— The orbit of a 0° libration amplitude, 0° inclination, $e = 0.24$ plutino in a frame that co-rotates with Neptune. The motion in the co-rotating frame is clockwise, except at perihelion, where this example’s e is so high that it briefly moves counter-clockwise. Pericenter occurs 90° ahead and behind Neptune’s position. Dotted circles are heliocentric distances of 30, 40, and 50 AU. Neptune’s position is shown for June 1, 2004 (which was midway through the CFEPS survey); this is true for all subsequent plots.

3.3. A realistic plutino distribution

In actuality, plutinos possess a range of libration amplitudes. Figure 5 shows an observationally-motivated distribution of plutinos, based on the debiased model from CFEPS (Gladman et al. 2012, excluding the Kozai component, which is discussed in detail in section 4). Chiang and Jordan (2002) and Malhotra (1996) also presented models of the plutino distribution. Malhotra (1996) discusses the dynamics of plutinos for given values of the libration amplitude, while Chiang and Jordan (2002) examined distributions of particles where A_{32} was established in a cosmogonic simulation. In contrast, our distributions of a , e , i , and ϕ_{32} are determined by debiasing the CFEPS Survey.

While at first glance it appears that the ‘turnaround’

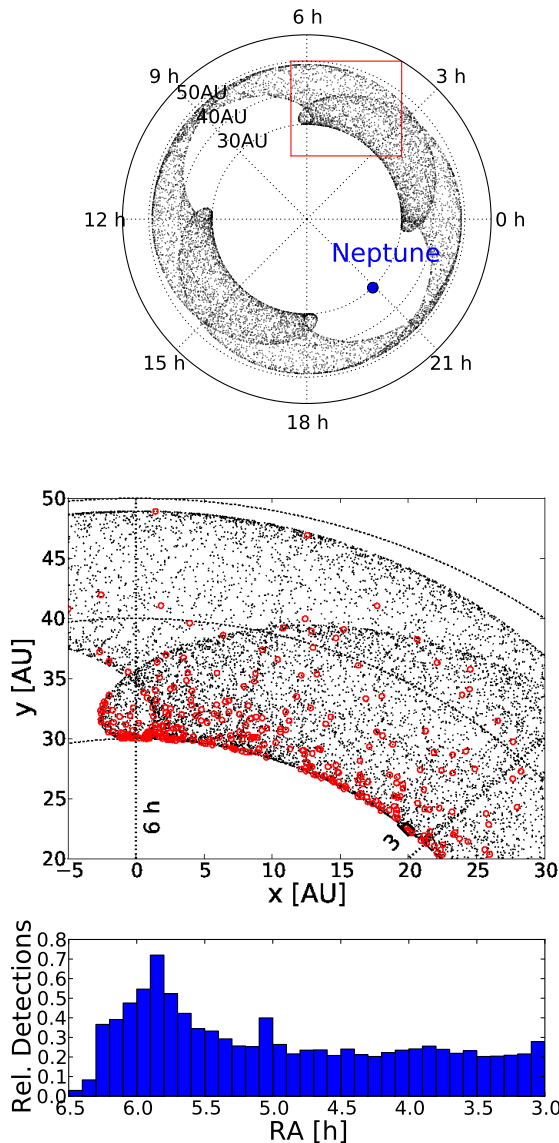


FIG. 4.— Top panel shows a population of plutinos with $A_{32} = 95^\circ$, $i = 0^\circ$, and $e = 0.24$ (see caption for Figure 3). The 95° libration amplitude means that the perihelion turnaround points correspond to orbits with perihelia 42.5° and 137.5° ahead and behind Neptune. The red box is shown at higher resolution in the middle panel, where red circles show simulated detections from a flux-limited all-sky survey. The lower panel shows that there are more detections per degree of ecliptic at the ‘turnaround’ point, which is where the libration causes the objects to come to pericenter farthest from the orthoneptune points. (The number of detections per bin is arbitrary.)

effect shown in Figure 4 is completely lost, this is not the case. Each plutino is still most likely to be detected at its maximum perihelion excursion from the orthoneptune points of $A_{32}/2$. So, a plutino with an 80° libration amplitude is most likely to be detected 40° away from the orthoneptune points, at $\lambda_N \pm 50^\circ$ or $\lambda_N \pm 130^\circ$, while a plutino with a 20° libration amplitude is most likely to be detected 10° away from the orthoneptune points, at $\lambda_N \pm 80^\circ$ or $\lambda_N \pm 100^\circ$.

Because CFEPS showed that plutinos with $A_{32} < 20^\circ$ are so rare as to be approximated as absent, two peaks in the detectability are visible, about 15° on either side of the orthoneptune points. As Figure 5 shows, this means

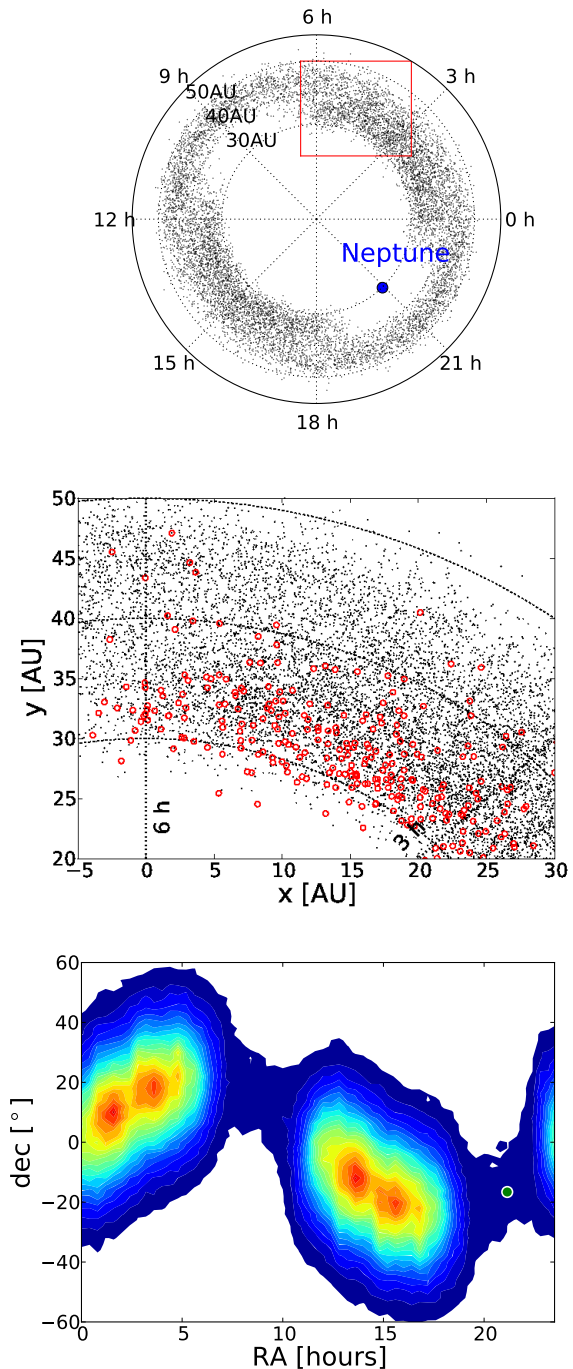


FIG. 5.— Top panel shows a population of plutinos with a distribution of orbital elements that matches the debiased plutino model from CFEPS (Gladman et al. 2012, excluding the Kozai component). See Figure 4 caption. The lower panel here shows the detection density on the sky, with red being higher density and blue being lower, with contours evenly spaced in detection density. Two peaks are visible on either side of the orthoneptune points, which are caused by the turnaround effect. At these peaks, the detection density is $\sim 30\%$ higher than at the orthoneptune points.

that the place on the sky to find the most plutinos is not 90° away from Neptune. For the CFEPS L7 model of the true libration amplitude distribution (Gladman et al. 2012), the maximum on-sky detection rate (integrated over all libration amplitudes) happens about $\pm 15^\circ$ away from the orthoneptune points.

4. KOZAI PLUTINO DYNAMICS

This section discusses the dynamics of objects that are simultaneously in the 3:2 mean-motion resonance with Neptune (plutinos) and in the Kozai resonance, and the effects these two simultaneous resonances have on the on-sky detectability.

The Kozai resonance can occur at much lower inclinations within mean-motion resonances than for non-resonant TNOs (Thomas and Morbidelli 1996; Wan and Huang 2007). The ω oscillation is unique to the Kozai resonance: the perturbations of the other solar system planets on a small body (resonant or not) normally cause ω to precess rather than librate.

The libration in e , i , and ω can be best understood using a contour plot of the averaged Hamiltonian of the disturbing function, which describes secular oscillation due to the three-body interaction. Example surfaces for the 4th order disturbing function for a Kozai plutino (Wan and Huang 2007) are shown in Figure 6. These are polar plots, where the length of the vector gives e , and the angle from 0° gives ω . In the cases shown, only the contours that close around 90° or 270° correspond to Kozai oscillations. Each plutino that is also in the Kozai resonance is confined to a particular contour on one of these surfaces. Tracing one contour reveals how e and ω vary during the course of a Kozai cycle, with the range in ω values describing the Kozai libration amplitude A_ω around the relevant libration center. Orbital inclination is calculated using e and conservation of the z-component of angular momentum $L_z \propto \cos i \sqrt{1 - e^2}$, because

$$\cos i \sqrt{1 - e^2} = \cos i_0 \sqrt{1 - e_0^2} \quad (5)$$

for initial inclination i_0 and initial eccentricity e_0 at any time. Each surface plot has its own L_z value, which is parameterized using I_{\max} :

$$\cos i_0 \sqrt{1 - e_0^2} = \cos I_{\max}$$

I_{\max} is the inclination required by conservation of angular momentum for $e=0$. Note that I_{\max} is not the maximum inclination that these plutinos will reach; in order for an object to have that inclination, it needs $e=0$, which will not happen in the course of a high- e Kozai oscillation. Plutinos always have maximum inclination values attained during their Kozai oscillations that are less than I_{\max} . I_{\max} is just a way to parameterize the level surfaces.

For a known Kozai plutino, the level surface can be chosen using the measured e_0 and i_0 values to calculate I_{\max} , which gives the Hamiltonian level surface for this object. The measured ω_0 value sets which contour the object is oscillating on, and knowing the contour allows the Kozai libration amplitude A_ω to be calculated numerically.

4.1. On-Sky Detection Biases for Kozai Plutinos

A direct consequence of the Kozai resonance-caused oscillation of ω is that these objects always come to pericenter out of the ecliptic plane. Because these are plutinos, we start with the same resonant condition (equation 3), and for this illustration choose $A_{32} = 0^\circ$:

$$\phi_{32} = 3\lambda - 2\lambda_N - \varpi$$

$$180^\circ = 3(\Omega + \omega + \mathcal{M}) - 2\lambda_N - (\Omega + \omega)$$

One can see from Figure 6 that when the Kozai libration amplitude is 0° , $\omega=90^\circ$ or 270° . At pericenter, $\mathcal{M} = 0^\circ$. Substituting these values into the above equation yields $\Omega = \lambda_N$, indicating that the node of the plutino orbit is in the same direction as Neptune, and ω will be 90° ahead or behind that position ($\Omega = \lambda_N + 180^\circ$ is also valid). The orbital plane of the plutino will be tilted out of the ecliptic plane by the inclination, with the line of nodes through Neptune’s position acting as the pivot. Most of the Kozai plutinos listed in the MPC database have orbital inclinations between 10° and 30° (Lykawka and Mukai 2007), which means that when they are at pericenter, a 0° Kozai libration amplitude plutino will be roughly $10-30^\circ$ above or below the ecliptic plane.

Solar System objects are most easily detected at pericenter, when they are closest and thus brightest. Because the Kozai plutinos are forced to be out of the ecliptic at pericenter, they will be harder to detect in ecliptic surveys than non-Kozai plutinos (see Figures 7 and 8). This is an important bias that must be accounted for.

5. SIMULATING THE PLUTINOS

We simulate the population of plutinos by randomly drawing from specified distributions of orbital elements and magnitudes, then taking each simulated plutino and “observing” it using the CFEPS survey simulator (publicly available at www.cfeeps.net). Figure 9 shows the simulated Plutino distribution in semimajor axis, eccentricity, and inclination. The non-Kozai plutino distribution we use here is identical to the CFEPS L7 model, while the Kozai plutino distribution here is more detailed than that used by Gladman et al. (2012).

The following describes how our code builds a population of plutinos with a realistic orbital element distribution, one simulated object at a time. The first step is to choose whether or not a given object is in the Kozai resonance or not.

An important parameter in these simulations is the true Kozai fraction $f_{\text{koz}}^{\text{true}}$, which is the true number of Kozai plutinos divided by the total number of plutinos. This is not necessarily the same as the observed Kozai fraction $f_{\text{koz}}^{\text{obs}}$, which is the total number of detected Kozai plutinos divided by the total number of detected plutinos for a given survey. For most of our simulations, we use a true Kozai fraction $f_{\text{koz}}^{\text{true}} = 10\%$, based on the results of CFEPS. However, because Gladman et al. (2012) found that Kozai fractions up to 33% cannot be ruled out at the 99% confidence level, some of our calculations are repeated for $f_{\text{koz}}^{\text{true}}$ values of 20% and 30%. Constraining the value of $f_{\text{koz}}^{\text{true}}$ will require many more well-characterized plutino detections than are currently available.

5.1. Non-Kozai Plutinos

For the plutinos which are *not* also in Kozai (with percentage $100\% - f_{\text{koz}}^{\text{true}}$), the following procedure is followed to choose its orbital elements. This is the same as the best-fit non-Kozai plutino model from CFEPS (Gladman et al. 2012).

First, the eccentricity is chosen from a Gaussian probability distribution centered on 0.18 with a width of 0.06. Eccentricities large enough to approach the orbit of Uranus ($e > 0.22$) are not allowed. The semi-major axis

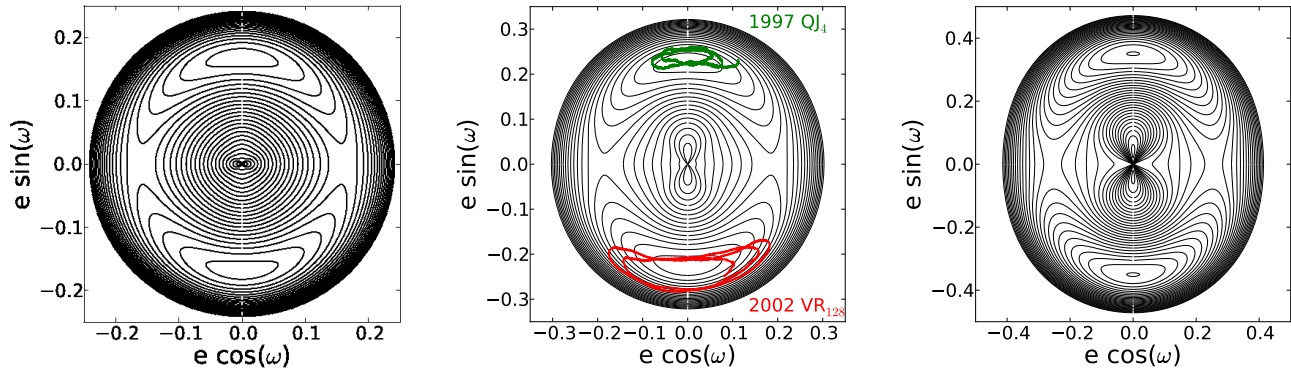


FIG. 6.— 3 different Hamiltonian level surfaces for plutinos (constructed using the disturbing function from Wan and Huang 2007), for different values of angular momentum. Left panel is $I_{\max} = 14^\circ$, center is $I_{\max} = 21^\circ$, and right is $I_{\max} = 34^\circ$. These are polar plots, with e as the radius and ω as the angle. Also shown on the center plot are the 10 Myr orbital integrations of the Kozai plutinos 1997 QJ₄ and 2002 VR₁₂₈, showing circulation around the $\omega = 90^\circ$ or 270° islands over time; these plutinos were chosen because they have $I_{\max} \approx 21^\circ$. While the presence of other planets causes small changes in the Hamiltonian, one can see that the evolution is decently approximated.

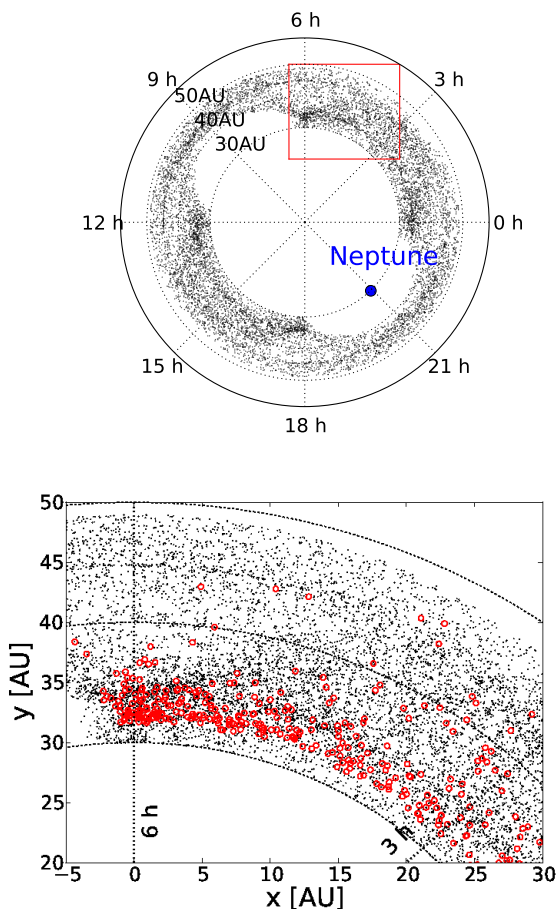


FIG. 7.— Top panel shows a toy model of the Kozai plutinos, where all objects have $A_{32} = 95^\circ$, using one contour from one level surface (meaning that all these Kozai plutinos have the same Kozai libration amplitude A_ω). Objects in the red box are shown at higher resolution in bottom panel. Red circles show simulated detections from a flux-limited ecliptic survey. The objects are only detected where they cross through the ecliptic plane, which is never when the objects are at pericenter.

is chosen from a simplified version of the stability tests of Tiscareno and Malhotra (2009). a is chosen within 0.2 AU of 39.45 AU for objects with $e > 0.15$. The allowed range of a values drops linearly as e gets smaller, reaching a width of zero at $e = 0$ (see Figure 9). The inclination is then chosen from a probability distribution of the form

$$P(i) \propto \sin i \exp\left(\frac{-i^2}{2\sigma_{32}^2}\right)$$

with $\sigma_{32} = 16^\circ$ (originally based on the inclination distribution postulated by Brown 2001). The libration amplitude is chosen from an asymmetric “tent-shaped” probability distribution with a peak at 95° , and linearly decreasing probabilities to the lower and upper bounds, 20° and 130° respectively, where the probability drops to zero.

Lastly, the object’s absolute magnitude H_g is chosen from an exponential distribution: $N(< H_g) \propto 10^{\alpha H_g}$, with $\alpha=0.9$. The reader is cautioned that this α value can only be considered valid in the range of H_g magnitudes where CFEPS had many detections (approximately $8 < H_g < 9$ for the plutinos). Sensitivity to the size distribution is discussed further in Section 6.3.

5.2. Kozai Plutinos

For a Kozai plutino, a slightly different path is followed to choose its orbital elements.

First, the Hamiltonian level surface is chosen. Inspecting the results of Lykawka and Mukai (2007), we found which Hamiltonian level surface corresponded to each of their Kozai plutinos. To reflect this distribution of surfaces, we used level surfaces corresponding to I_{\max} of 14° , 16° , 17.5° , 20° , 21° , 21.3° , 21.6° , 22.5° , 24° , 26° , 28° , and 34° , in equal proportions. In reality, due to the historical dominance of ecliptic surveys and the bias against detecting large i TNOs, there are probably a larger fraction of large i Kozai librators; however, the currently available information does not justify more complex modeling.

Once the I_{\max} level surface is chosen, we pick a Kozai libration amplitude A_ω at random between 10° - 80° . ω is then chosen sinusoidally within the values allowed by

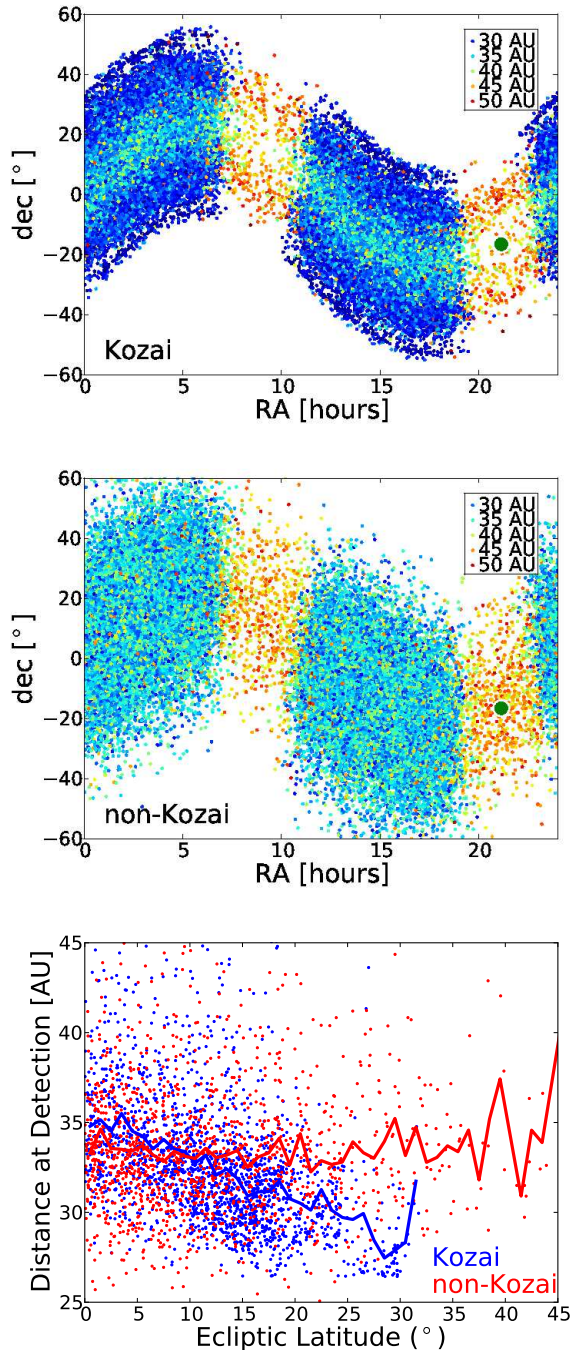


FIG. 8.— Detected plutinos in a simulated, flux-limited, all-sky survey, using realistic distributions for both populations. In the two upper panels, the color of each point shows the distance at which the plutino was detected (see legend in panels), with Kozai plutinos in the uppermost panel and non-Kozai plutinos in the middle panel. The non-Kozai plutinos are detected at a broad distance range in each of the two pericenter lobes. The distance at which the Kozai plutinos are detected is very much dependent on ecliptic latitude, with higher ecliptic latitudes detected at closer distances, and lower detected at greater distances. The large green dot marks Neptune’s location. The lower panel shows the distance and ecliptic latitude where each plutino was detected, using one of the pericenter lobes (plutinos between ecliptic longitudes of 12h–18h). Blue shows Kozai plutinos, red shows non-Kozai. The solid lines show the average in 0.5° bins of ecliptic latitude. The average detection distance for Kozai plutinos depends on ecliptic latitude, with those at low latitudes being at the farthest average heliocentric distance. Non-Kozai plutinos show no such trend.

A_ω . Because of the banana-shape of the contours, there are two values of e allowed for any given value of ω (see Figure 6). Given this value of ω , the Wan and Huang (2007) disturbing function allows numerical determination of the two e values that correspond to ω on the contour. Half of the time we choose the lower value of e , and half higher. The inclination i is calculated using $\cos i\sqrt{1-e^2} = \cos I_{\max}$. Since this only covers the 90° Kozai libration island, half of the objects are flipped ω of to 360° minus the original ω value.

Lastly, the semi-major axis, the libration amplitude A_{32} , and the absolute H magnitude are all chosen following the same procedure as for the non-Kozai plutinos.

6. ON-SKY BIASES

We build up a population of synthetic plutinos, drawing orbital elements and magnitudes from the specified distributions as described above, and determine if each object is detected by a survey using the survey simulator code. Using the specified field coverage, magnitude efficiency, and tracking fraction, the code determines whether or not each object will be detected by the survey. Comparing the distributions of the drawn and simulator-detected objects gives an idea of the biases that are present in surveys that cover different areas of the sky to different magnitude depths. When the simulated detections are compared to the true detections in a real, well-characterized survey, this is a powerful tool to help in debiasing to regain the real intrinsic population’s orbital distribution.

Figure 10 shows an on-sky detection density map for all the plutinos, including the Kozai component. With the Kozai component included, it is still true that most plutinos are detected in broad clumps around the orthon Neptune points, 90° away from Neptune. The reader will notice that the highest detection densities still occur in clumps in the ecliptic on either side of the orthon Neptune points rather than exactly centered on the orthon Neptune points. This is caused by the “turnaround” detection effect described in Section 3.3.

The Kozai plutinos are only visible (for this realistic model) as subtle density enhancements about 10° off the ecliptic, making the density contours in Figure 10 appear slightly more rectangular than in Figure 5. This rectangular shape is enhanced for higher values of $f_{\text{koz}}^{\text{true}}$. Note that there is no “spike” in detections at the ecliptic latitudes where the density of Kozai plutinos is highest; the detection densities are still dominated by the much greater numbers of non-Kozai plutinos.

To clarify what is happening for the Kozai population, the Kozai component is shown separately in Figure 11. The Kozai plutino detections are more confined in ecliptic latitude than the non-Kozai plutinos, with the highest detection densities happening about 10° above and below the ecliptic, in broad swaths surrounding the orthon Neptune points, with the central minimum again caused by the lack of $A_{32} < 20^\circ$ plutinos.

6.1. Ecliptic Latitude Distribution of Detections

Figure 12 presents the ecliptic latitudes of detected Plutinos in a simulated all-sky survey. The number of detections for all plutinos smoothly falls from 0° ecliptic latitude on up to higher latitudes. Although the number of Kozai detections climbs as one rises to $\sim 15^\circ$ ecliptic

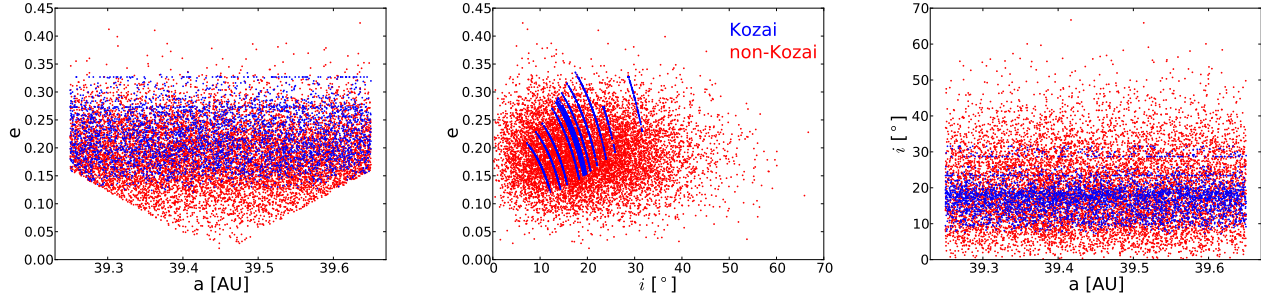


FIG. 9.— Distribution of simulated plutinos in semimajor axis, eccentricity, and inclination. Red points are non-Kozai plutinos and blue points are plutinos in the Kozai resonance. The Kozai plutinos are constrained by the conservation of L_z and our choice of I_{\max} values. This is especially obvious in the middle panel, where each Kozai curve corresponds to a particular I_{\max} value; over a Kozai libration cycle, objects never reach $e = 0$, and thus always have $i < I_{\max}$.

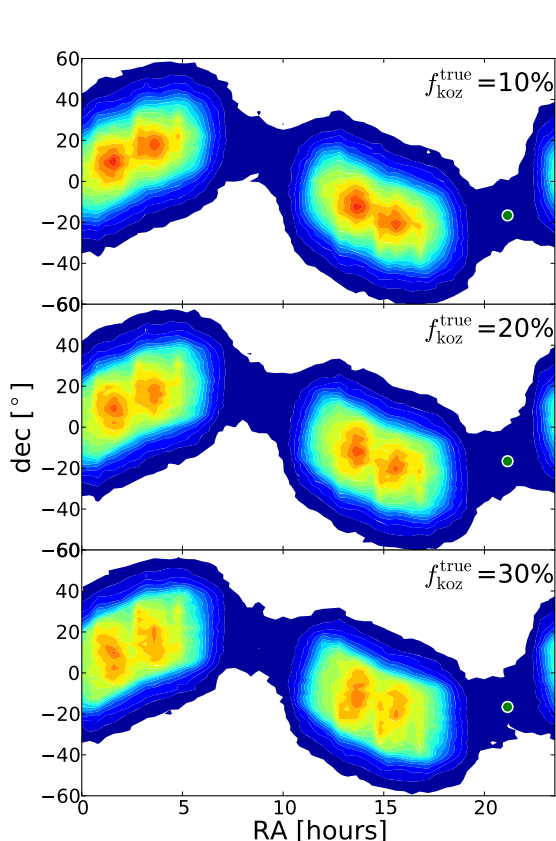


FIG. 10.— Relative density of detections on the sky in an all-sky survey using our plutino model, including both Kozai and non-Kozai components, for three different values of $f_{\text{koz}}^{\text{true}}$. Contours are evenly spaced in detection density, and contour values are the same in all three plots (absolute detection densities are arbitrary). The position of Neptune is shown by a green circle. The detection density becomes somewhat less concentrated to the ecliptic for increasing Kozai fraction.

latitude, they never hold more than about half the detections in a bin.

Schwamb et al. (2010) and Brown (2008) found a factor of ~ 4 spike in the number of detections in their surveys in the $11\text{--}13^\circ$ ecliptic latitude bin, which they attribute to potentially being caused by Kozai plutinos. However, our simulation makes this explanation implausible. Even when we go to the extreme and unrealistic

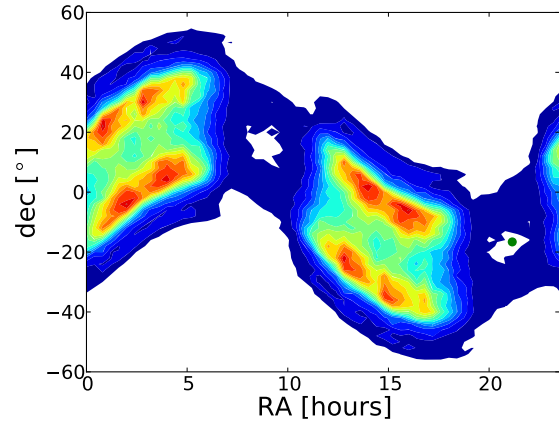


FIG. 11.— Relative density of detections on the sky using an all-sky survey only using the Kozai component of our model. Contours are evenly spaced in detection density. The position of Neptune is shown by a green circle.

case of only using the lowest I_{\max} value of 14° (which makes the Kozai plutinos as compact as possible in ecliptic latitude), and using the highest value of $f_{\text{koz}}^{\text{true}} = 30\%$, we still find that there is only a $\sim 20\%$ increase in the number of plutinos at ecliptic latitudes of $11\text{--}13^\circ$. Kozai plutinos do not explain this spike in detections, because it is impossible to confine the detections of Kozai librators to a narrow ecliptic latitude bin. The reported detection spike is likely a small-number statistics fluctuation.

6.2. f_{koz} On-Sky

Figure 13 shows the ratio between the number of Kozai plutino detections to the total number of plutino detections in small bins on the sky, providing a local $f_{\text{koz}}^{\text{obs}}$ map. (This is essentially the ratio of Figure 11 to Figure 10). Figure 13 shows the range of $f_{\text{koz}}^{\text{obs}}$ values that could be locally found at different positions on the sky, for $f_{\text{koz}}^{\text{true}}$ of 10%, 20%, and 30%.

$f_{\text{koz}}^{\text{obs}}$ values vary from 0% to nearly twice the $f_{\text{koz}}^{\text{true}}$ values. The highest $f_{\text{koz}}^{\text{obs}}$ values occur where the Kozai detection density is highest: above and below the ecliptic plane by about 12°

6.3. Size Distribution Effects

The diameter distribution of TNOs is fit by a power law, usually parameterized as $N(> d) \propto d^{-Q}$, where $N(> d)$ is the number of objects larger than a diameter d , and Q is the index of the power law. However,

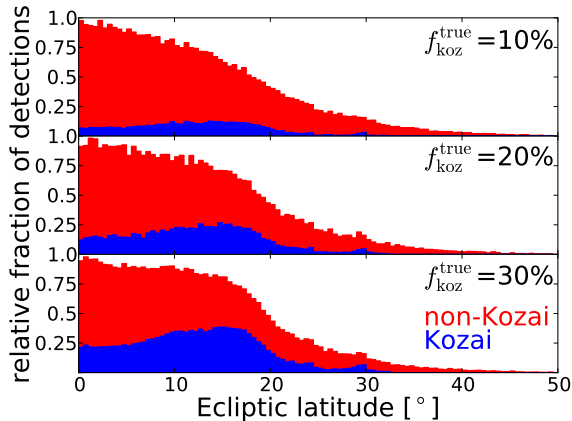


FIG. 12.— Stacked histograms of the ecliptic latitude distribution of detected Plutinos for different values of $f_{\text{koz}}^{\text{true}}$, using a magnitude-limited all-sky survey. The number of detections per bin is normalized to the maximum bin. Kozai plutinos are shown in red, non-Kozai plutinos in blue.

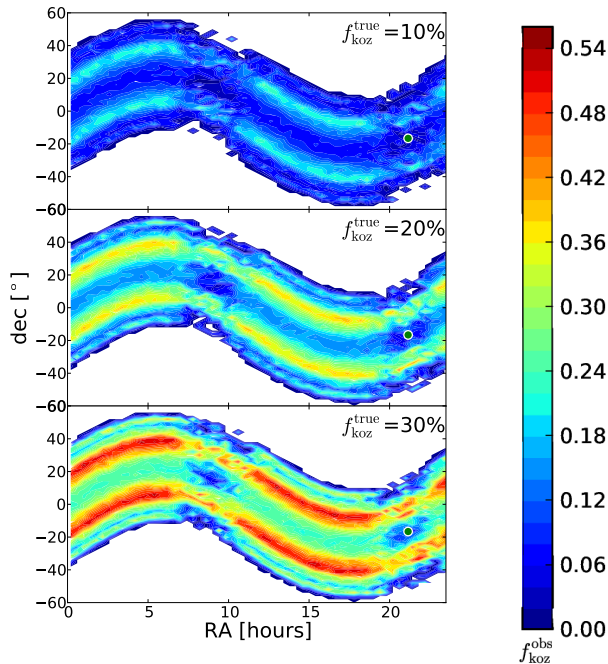


FIG. 13.— This shows $f_{\text{koz}}^{\text{obs}}$, the number of Kozai plutino detections divided by the total number of plutino detections in $2^\circ \times 6^\circ$ bins on the sky, using our best plutino model. The true Kozai fraction (for the entire plutino population) $f_{\text{koz}}^{\text{true}}$, is 10% in the top panel, 20% in the center, and 30% in the lower panel. The local $f_{\text{koz}}^{\text{obs}}$ varies widely, from nearly zero around Neptune to its highest values about 10° off the ecliptic.

because only a few of the largest KBOs have had their diameters directly measured by occultation or resolved imaging, what is actually measured is the magnitude. To convert this to a diameter, an albedo must be measured or assumed. For this reason we discuss the size distribution in terms of absolute magnitude: $N(< H) \propto 10^{\alpha H}$. The values Q and α are related: $\alpha = \frac{Q}{5}$.

The logarithmic slope α is known to be dif-

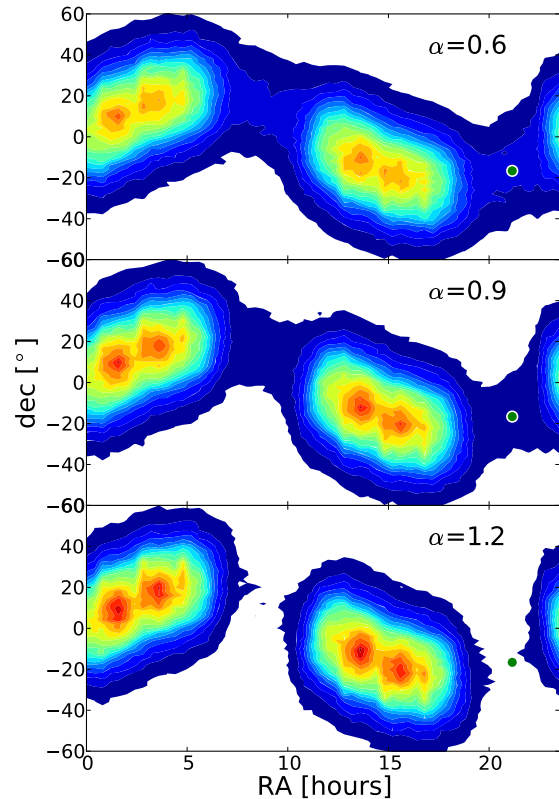


FIG. 14.— Relative density of plutino detections (including Kozai, with $f_{\text{koz}}^{\text{true}} = 10\%$) using three different values of α , the logarithmic slope of the size distribution in absolute magnitude. Contours are evenly spaced in detection density, and the contours represent the same values in each panel. For steeper power laws, the density of detection also becomes steeper, with more detections at the turnaround points, and fewer detections 90° away.

ferent depending on the size of the KBOs (e.g. Fuentes and Holman 2008; Fraser and Kavelaars 2009). For most of our calculations, we use the nominal CFEPS value for plutinos of $\alpha = 0.9$ (Gladman et al. 2012). But for comparison, Figure 14 shows the effect of different values of α on the detection density, and Figure 15 shows the effect of different α values on $f_{\text{koz}}^{\text{obs}}$ at different places on the sky. Steeper slopes result in steeper detection density distributions, where the peak detection densities are much higher. This is because the relative importance of detecting the large number of small plutinos that are only visible at perihelion increases. Lower values of α result in shallower density distributions. This effect is noticeable, but the overall pattern of where on the sky the highest $f_{\text{koz}}^{\text{obs}}$ values are remains the same.

6.4. Example Simulated Surveys

We perform a number of strawman simulated surveys to demonstrate the different values of apparent average $f_{\text{koz}}^{\text{obs}}$ that result from different survey parameters and different $f_{\text{koz}}^{\text{true}}$ values. These are summarized in Table 1. For all of these simulated surveys, we ignore the extra confusion caused by the plane of the Milky Way, and assume that the entire area within each survey is observed uni-

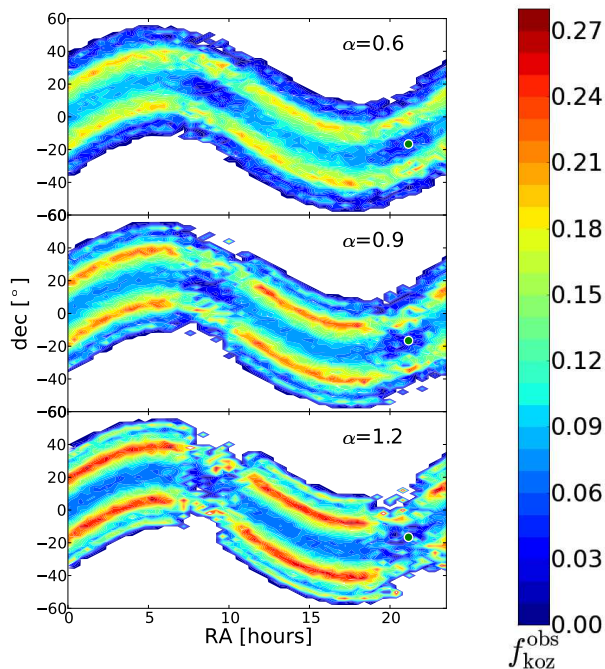


FIG. 15.— $f_{\text{koz}}^{\text{obs}}$ at different points on the sky, using $f_{\text{koz}}^{\text{true}} = 10\%$, and three different slopes for the power-law absolute magnitude distribution. Steeper slopes cause the $f_{\text{koz}}^{\text{obs}}$ value to vary more widely, reaching maximum values of almost 30%, while the shallow slopes give the highest $f_{\text{koz}}^{\text{obs}}$ values of only about 20%.

formly and with perfect tracking efficiency (that is, all discoveries are tracked to yield high quality orbits).

Each simulated survey goes to a magnitude depth of $g = 24.9$. Varying the magnitude depth did not have any noticeable effect on the detection density or f_{koz} values on the sky, due to the assumed exponential nature of the distribution.

First we perform an all-sky survey with a set limiting magnitude (Survey 1), which finds a higher Kozai fraction than reality, with $f_{\text{koz}}^{\text{obs}}$ being higher than $f_{\text{koz}}^{\text{true}}$. Survey 2, an ecliptic survey covering the entire ecliptic within $\pm 2.5^\circ$, unsurprisingly finds the opposite effect, with $f_{\text{koz}}^{\text{obs}}$ being lower than $f_{\text{koz}}^{\text{true}}$. This is due to the Kozai plutinos preferentially being detected out of the ecliptic plane, as discussed in Section 4.1.

Surveys 3 and 4 are $20^\circ \times 20^\circ$ surveys centered on the ecliptic. Survey 3 is centered 90° away from Neptune, and Survey 4 is centered 75° away from Neptune, near the plutinos' peak in detectability. Surveys 5 and 6 are smaller, $2^\circ \times 2^\circ$ surveys, centered on the ecliptic 90° and 75° away from Neptune, respectively. These four surveys all find lower $f_{\text{koz}}^{\text{obs}}$ than $f_{\text{koz}}^{\text{true}}$, for the same reason as Survey 2.

Surveys 7 and 8 are the same as Surveys 3 and 4, except centered 10° above the ecliptic. Similarly, Surveys 9 and 10 are the same as Surveys 5 and 6, raised to 10° above the ecliptic. Because these surveys cover the range of the Kozai plutinos' peak detection density, they all find higher $f_{\text{koz}}^{\text{obs}}$ than $f_{\text{koz}}^{\text{true}}$ values.

There is not a significant difference between the $f_{\text{koz}}^{\text{obs}}$ values measured by the surveys that are centered on 90° from Neptune and those centered on 75° from Neptune.

There *is* a difference in the relative number of detections, with overall more plutinos detected at 75° from Neptune. However, because both the Kozai and non-Kozai plutinos have the same A_{32} distribution in this model, the Kozai fraction does not vary significantly between these two positions on the sky.

These surveys demonstrate that very different values of $f_{\text{koz}}^{\text{obs}}$ can be measured depending on the on-sky location of the survey. Due to the different biases inherent in the distribution of Kozai plutinos versus non-Kozai plutinos, careful debiasing is required to calculate $f_{\text{koz}}^{\text{true}}$ from any survey, even one which covers the entire sky.

7. COMPARISON WITH PREVIOUS LITERATURE

In the previous sections, we have discussed two quantities that can be measured for a survey or simulation that contains many well-characterized plutinos: f_{koz} and the distribution of I_{max} for the Kozai plutinos. Below, we discuss these quantities as measured by observational surveys and giant planet migration simulations. Only a few surveys are discussed here, as only a few previously published TNO surveys have rigorous enough tracking and characterization methods to classify plutinos as Kozai or non-Kozai in orbital integrations.

7.1. The Kozai Fraction f_{koz}

The simplest quantity to measure in a survey or simulation that contains plutinos is f_{koz} , the fraction of plutinos that are in Kozai. However, one must be careful to note whether this is the true or apparent f_{koz} . Most surveys will have some bias, as shown in Table 1, causing $f_{\text{koz}}^{\text{obs}}$ to be different than $f_{\text{koz}}^{\text{true}}$.

Below we discuss the f_{koz} results presented in several observational surveys and theoretical simulations. A summary is presented in Table 2.

7.1.1. Observational Surveys: $f_{\text{koz}}^{\text{obs}}$

CFEPS (Petit et al. 2011), being a well-calibrated survey, was able to provide both an apparent and a true f_{koz} , albeit with large uncertainty (Gladman et al. 2012). They find $f_{\text{koz}}^{\text{obs}}$ of $2/24 = 8\%$. After debiasing, this would require a value of $f_{\text{koz}}^{\text{true}}$ of 10%. However, because CFEPS was confined to the ecliptic plane, it was not very sensitive to the high-inclination Kozai plutino population, and $f_{\text{koz}}^{\text{true}}$ up to 33% cannot be ruled out with 99% confidence due to the small number statistics of having only two detected Kozai plutinos.

The Deep Ecliptic Survey (Elliot et al. 2005), while finding a reported 51 plutinos, did not specifically label any of their discovered plutinos as Kozai, and thus is not discussed further (although some of their discoveries are in the biased Lykawka and Mukai (2007) compilation, discussed below).

A few papers have tried to use the entire MPC database as a survey. While this does provide many plutinos, the MPC contains the results of many surveys and even serendipitous discoveries, each with completely different and possibly unknown biases, since one doesn't know where searches failed to detect plutinos. Debiasing $f_{\text{koz}}^{\text{obs}}$ to find $f_{\text{koz}}^{\text{true}}$ is impossible for these surveys.

Gomes (2000) and Nesvorný et al. (2000) performed similar large MPC database searches capable of classifying objects as Kozai or non-Kozai plutinos. Gomes

TABLE 1
SIMULATIONS OF f_{koz}

Survey Description	f_{koz}^{obs} values for:		
	$f_{koz}^{true} = 10\%$	$f_{koz}^{true} = 20\%$	$f_{koz}^{true} = 30\%$
1 all sky	12 %	23 %	35 %
2 5° high, on ecliptic	7.5 %	15 %	23 %
3 20°×20° box, 90° from Neptune, on ecliptic	9.5 %	19 %	29 %
4 20°×20° box, 75° from Neptune, on ecliptic	10 %	18 %	28 %
5 2°×2° box, 90° from Neptune, on ecliptic	7.6 %	16 %	24 %
6 2°×2° box, 75° from Neptune, on ecliptic	7.4 %	16 %	23 %
7 20°×20° box, 90° from Neptune, 10° off ecliptic	13 %	25 %	37 %
8 20°×20° box, 75° from Neptune, 10° off ecliptic	13 %	24 %	36 %
9 2°×2° box, 90° from Neptune, 10° off ecliptic	14 %	26 %	37 %
10 2°×2° box, 75° from Neptune, 10° off ecliptic	14 %	27 %	38 %

TABLE 2
MEASUREMENTS OF f_{koz} FROM THE LITERATURE

Source	type	f_{koz}^{true}	f_{koz}^{obs}	# plutinos
Gomes (2000)	Observational	-	26%	23
Nesvorný et al. (2000)	Observational	-	12%	33
Chiang and Jordan (2002)	Theoretical	20-30%	-	42
Hahn and Malhotra (2005)	Theoretical	19%	-	133
Lykawka and Mukai (2007)	Observational	-	22-30%	100
Levison et al. (2008)	Theoretical	16%	-	186
Schwamb et al. (2010)	Observational	-	33%	6
Gladman et al. (2012)	Observational	10%	8%	24

(2000) examined the first 23 discovered Plutinos with observations for 2 or more oppositions. Though many of these classifications were provisional due to a lack of precise data, he found f_{koz}^{obs} of $6/23 = 26\%$. Nesvorný et al. (2000) performed a similar analysis for the first 33 plutinos, finding that only 4 of them were in Kozai, giving f_{koz}^{obs} of 12%, despite an overlapping sample.

Currently, the largest collection of well-classified plutinos was presented in Lykawka and Mukai (2007), with 100 plutinos from the MPC database. All of these plutinos had at least 2 opposition observations, and 10 Myr orbital integrations were performed. They found that 22 plutinos are solidly in the Kozai resonance, with 8 more that are in the Kozai resonance for part of their integration. Thus, from their integrations they find f_{koz}^{obs} of 22-30%.

Schwamb et al. (2010) completed a wide-field survey covering a large fraction of the sky ($\sim 12,000$ square degrees) within 30° of the ecliptic. This relatively shallow survey ($R \sim 21.5$) found 6 plutinos, two of which are in Kozai, giving $f_{koz}^{obs} = 33\%$, albeit with large Poisson uncertainty. The higher ecliptic latitudes included in this survey would make detecting the Kozai plutinos more likely, thus this higher apparent f_{koz}^{obs} value is not surprising. Although this is the first large area survey which found and tracked plutinos and Kozai plutinos, a much larger number of plutino detections will be needed to accurately measure the Kozai fraction.

7.1.2. Theoretical Simulations: f_{koz}^{true}

Of the published simulations of giant planet migration, only Chiang and Jordan (2002) includes information on which plutino test particles ended up in Kozai. Future simulations should include this information, as

it may prove a useful diagnostic. We also discuss the Kozai plutinos from Hahn and Malhotra (2005) and Levison et al. (2008), because the authors provided us with the output orbits of these simulations and were able to complete the required analysis ourselves.

Chiang and Jordan (2002) studied a smooth outward migration of Neptune, with different migration times for Neptune to reach its current location. They discuss objects that are captured into the Kozai resonance within the 3:2 for their simulation where Neptune migrates with a damping half-life of 10^7 years. Because of the shorter timescale of their simulations, their resonance classification isn't as secure as in the other simulations discussed below. Out of 92 plutinos at the end of their simulation, they estimate that 42 will remain in the 3:2 resonance for the age of the solar system. Of these, 8-12 are in Kozai, giving f_{koz}^{true} of 20-30%. They unfortunately do not discuss the effect that different migration timescales have on the Kozai fraction, nor how f_{koz}^{true} might evolve over 4 Gyr.

Hahn and Malhotra (2005) and Levison et al. (2008) provided enough data from the end of their theoretical migration simulations that we were able to continue the integrations for 10 Myr, long enough to diagnose if a plutino is in Kozai or not. Hahn and Malhotra (2005) used a smooth outward migration of Neptune, while Levison et al. (2008) had Neptune on a large-eccentricity orbit that damps after interacting with the Kuiper Belt (motivated by the ‘‘Nice Model’’ scenario; Tsiganis et al. 2005).

For the Levison et al. (2008) simulation, we were given the 10 Myr orbital integrations originally used to classify objects as resonant or non-resonant at the end of their 1 Gyr migration simulation (Run B). These integrations

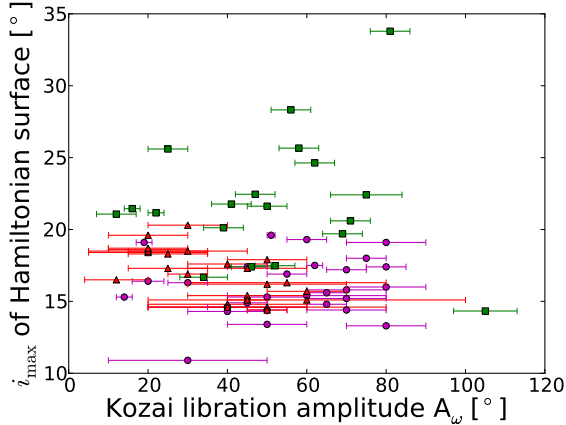


FIG. 16.— Scatterplot showing the I_{\max} values (which parameterize which Hamiltonian level surface the plutino is on), and the Kozai libration amplitudes A_ω (which parameterizes which contour of the level surface the plutino is on). Purple circles show simulated Kozai plutinos from Levison et al. (2008) (LMVGT2008), green squares show real Kozai plutinos from the MPC database (L&M2007, Lykawka and Mukai 2007), and red triangles show simulated Kozai plutinos from Hahn and Malhotra (2005) (H&M2005). Error bars for the MPC values are those reported by Lykawka and Mukai (2007), other error bars are estimated by eye from orbital integrations.

contain the osculating orbital elements at each timestep, and these were searched for oscillation of ω around 90° or 270° to determine A_ω .

For the Hahn and Malhotra (2005) data, we were provided the osculating orbital elements of all test particles and the 4 giant planets at the end of their 4.5 Gyr giant planet migration simulation. However, these were divided into 100 separate simulations, each with different giant planet positions and different numbers of remaining test particles (most had ~ 50). Each of these were input into a slightly modified version of the orbital integrator SWIFT (Levison and Duncan 1994), and 30 Myr orbital integrations were performed. We analysed the remaining test particles for libration of ϕ_{32} , and then for oscillation of ω around 90° or 270° .

Out of 133 plutinos in the Hahn and Malhotra (2005) simulation, 25 were in Kozai, giving $f_{\text{koz}}^{\text{true}} = 19\%$. The Levison et al. (2008) simulation provided 186 plutinos, of which 29 were in Kozai, giving $f_{\text{koz}}^{\text{true}} = 16\%$.

These f_{koz} values all contain large uncertainties, and in our opinion, all roughly agree with each other at this point. As more plutinos are found by rapidly repeating all-sky surveys such as LSST, the value of $f_{\text{koz}}^{\text{true}}$ should become precisely measurable as the survey characterization becomes well-determined.

7.2. Distribution of Kozai Parameters

The two main parameters we use to describe the Kozai behavior of a given Kozai plutino are I_{\max} and the Kozai libration amplitude A_ω . The distribution of I_{\max} tells about the range of e and i that are possible during a Kozai cycle. I_{\max} is a parameterization of which Hamiltonian level surface currently best describes the Kozai libration of that plutino. The Kozai libration amplitude A_ω measures which contour within the I_{\max} level surface the plutino is on, and is found from looking at the results of a 10-30 Myr diagnostic orbital integration.

Because this is a distribution and not just a sin-

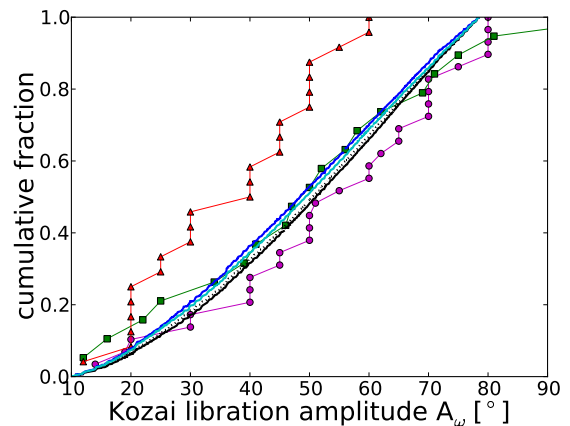
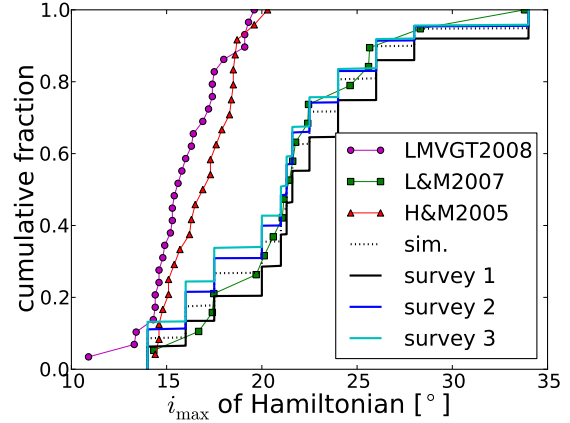


FIG. 17.— Cumulative distributions of I_{\max} and A_ω values. See Figure 16 caption for symbols. The intrinsic distribution of thousands of simulated Kozai plutinos using our model is shown by a dotted black line. The results of running this distribution through a survey simulator using parameters for Surveys 1, an all-sky survey, Survey 2, an ecliptic survey, and Survey 3, a $20^\circ \times 20^\circ$ survey centered 90° from Neptune (see Section 6.4) are shown by solid lines. The models produce generically lower inclination objects, but seem to produce similar Kozai libration amplitudes to the MPC objects (keep in mind that the MPC objects are not debiased). Note that the intrinsic model matches the MPC sample quite well because, as explained in Section 5.2, the distribution of Kozai I_{\max} values was based on the objects in the MPC.

gle value like f_{koz} , it is only instructive to analyse for the surveys and simulations with the largest number of plutinos. We compare the I_{\max} distributions found in the theoretical giant planet migration simulations of Hahn and Malhotra (2005) and Levison et al. (2008) with the MPC database analysis presented in Lykawka and Mukai (2007), and with our own simulation (Figures 16 and 17).

When looking at Figures 16 and 17, it is important to keep in mind that we are comparing different kinds of distributions. The simulated Kozai plutinos from Levison et al. (2008), Hahn and Malhotra (2005), and this paper are intrinsic distributions, that is, not observed by a biased survey. The MPC-detected Kozai plutinos (from Lykawka and Mukai 2007) and the distributions resulting from the simulated surveys presented in this paper are biased. In the case of the MPC sample, which contains the results of many uncharacterized surveys, precise debiasing is impossible. The simulated

surveys, however, are all based on our simulated plutino distribution, so we can see the effects of different types of surveys on the detected parameters. The all-sky survey (Survey 1) is slightly biased toward finding a higher proportion of higher I_{\max} objects than reality, while Surveys 2 and 3 are weakly biased toward finding a higher proportion of lower I_{\max} objects than reality. All three simulated surveys show little bias in the distribution of Kozai libration amplitudes.

The distribution of Kozai libration amplitudes is shown in the bottom panel of Figure 17. There is general agreement between libration amplitude distribution of the MPC Kozai plutinos and both giant planet migration simulations, however, the Hahn and Malhotra (2005) simulation finds generally lower libration amplitudes, while the Levison et al. (2008) simulation finds generally higher. This is an area that could use more theoretical work, as different migration timescales and migration modes may cause different libration amplitude distributions.

It is obvious from the top panel of Figure 17 that the I_{\max} values are much lower in both of the simulations than in the MPC. Although the MPC distribution is not debiased, and thus may not reflect the true distribution of Kozai plutinos, the inclination distribution discrepancy between models and the true Kuiper Belt has been noticed before (Gladman et al. 2012). This is a generic problem with giant planet migration simulations, and not unique to this Kozai problem: these simulations are not good at raising the inclinations of the captured resonant objects (noted by Chiang and Jordan 2002, and others).

8. CONCLUSION

With the upcoming inauguration of such rapid-fire all-sky surveys as LSST (LSST Science Collaboration et al. 2009; Jones et al. 2009) and Pan-STARRS (Grav et al.

2011), which are expected to detect hundreds of new TNOs, we are entering an era when we have enough well-characterized plutinos to be able to debias and measure the value of $f_{\text{koz}}^{\text{true}}$ with more precision than has been possible.

Little theoretical work has been done relating the value of $f_{\text{koz}}^{\text{true}}$ to the migration timescale of Neptune, but this may be an important and helpful diagnostic. To our knowledge, no theoretical work has been done so far to understand how the I_{\max} distribution is set, and how it evolves over time. There are also other relationships that have not been explored, such as the relation between the libration amplitude of ϕ_{32} and the Kozai libration amplitude.

Our results allows optimization for observers planning targeted surveys. If the goal of the survey is to find as many plutinos as possible, the highest density on the sky is not exactly 90° away from Neptune, but about 15° on either side of $\lambda_N \pm 90^\circ$. If the goal of the survey is to find as many Kozai plutinos as possible, the best places on the sky are about 12° above and below the ecliptic, and 15° on either side of the orthoneptune points. The value of $f_{\text{koz}}^{\text{obs}}$ that is measured in a given survey can be significantly different from $f_{\text{koz}}^{\text{true}}$, and careful debiasing is necessary to derive the true value. Parameters of the survey such as pointings, field depths, tracking efficiencies, and fields with no detections must all be characterized in order to properly debias the results (see Jones et al. 2010).

The authors wish to thank C. Van Laerhoven, H. Levison, and J. Hahn for providing us with output from their migration simulations, and X.-S. Wan and T.-Y. Huang for providing us with the disturbing function coefficients for Kozai plutinos.

REFERENCES

- Brown, M. E.: 2001, *AJ* **121**, 2804
 Brown, M. E.: 2008, *The Largest Kuiper Belt Objects*, pp 335–344
 Chiang, E. I. and Jordan, A. B.: 2002, *AJ* **124**, 3430
 Cohen, C. J. and Hubbard, E. C.: 1964, *Science* **145**, 1302
 Davies, J. K., McFarland, J., Bailey, M. E., Marsden, B. G., and Ip, W.-H.: 2008, *The Early Development of Ideas Concerning the Transneptunian Region*, pp 11–23
 Elliot, J. L., Kern, S. D., Clancy, K. B., Gulbis, A. A. S., Millis, R. L., Buie, M. W., Wasserman, L. H., Chiang, E. I., Jordan, A. B., Trilling, D. E., and Meech, K. J.: 2005, *AJ* **129**, 1117
 Fraser, W. C. and Kavelaars, J. J.: 2009, *AJ* **137**, 72
 Fuentes, C. I. and Holman, M. J.: 2008, *AJ* **136**, 83
 Gallardo, T., Hugo, G., and Pais, P.: 2012, *Icarus* **220**, 392
 Gladman, B., Lawler, S. M., Petit, J.-M., Kavelaars, J., Jones, R. L., Parker, J. W., Van Laerhoven, C., Nicholson, P., Rousset, P., Bieryla, A., and Ashby, M. L. N.: 2012, *AJ* **144**, 23
 Gladman, B., Marsden, B. G., and Vanlaerhoven, C.: 2008, *Nomenclature in the Outer Solar System*, pp 43–57
 Gomes, R. S.: 2000, *AJ* **120**, 2695
 Grav, T., Jedicke, R., Denneau, L., Chesley, S., Holman, M. J., and Spahr, T. B.: 2011, *PASP* **123**, 423
 Hahn, J. M. and Malhotra, R.: 2005, *AJ* **130**, 2392
 Jones, R. L., Chesley, S. R., Connolly, A. J., Harris, A. W., Ivezić, Z., Knežević, Z., Kubica, J., Milani, A., and Trilling, D. E.: 2009, *Earth Moon and Planets* **105**, 101
 Jones, R. L., Gladman, B., Petit, J.-M., Rousset, P., Mousis, O., Kavelaars, J. J., Campo Bagatin, A., Bernabeu, G., Benavidez, P., Parker, J. W., Nicholson, P., Holman, M., Grav, T., Doressoundiram, A., Veillet, C., Scholl, H., and Mars, G.: 2006, *Icarus* **185**, 508
 Jones, R. L., Parker, J. W., Bieryla, A., Marsden, B. G., Gladman, B., Kavelaars, J., and Petit, J.-M.: 2010, *AJ* **139**, 2249
 Kavelaars, J. J., Jones, R. L., Gladman, B. J., Petit, J., Parker, J. W., Van Laerhoven, C., Nicholson, P., Rousset, P., Scholl, H., Mousis, O., Marsden, B., Benavidez, P., Bieryla, A., Campo Bagatin, A., Doressoundiram, A., Margot, J. L., Murray, I., and Veillet, C.: 2009, *AJ* **137**, 4917
 Kozai, Y.: 1962, *AJ* **67**, 591
 Levison, H. F. and Duncan, M. J.: 1994, *Icarus* **108**, 18
 Levison, H. F., Morbidelli, A., Vanlaerhoven, C., Gomes, R., and Tsiganis, K.: 2008, *Icarus* **196**, 258
 LSST Science Collaboration, Abell, P. A., Allison, J., Anderson, S. F., Andrew, J. R., Angel, J. R. P., Armus, L., Arnett, D., Asztalos, S. J., Axelrod, T. S., and et al.: 2009, *ArXiv e-prints*
 Lykawka, P. S. and Mukai, T.: 2007, *Icarus* **189**, 213
 Malhotra, R.: 1996, *AJ* **111**, 504
 Nesvorný, D. and Roig, F.: 2000, *Icarus* **148**, 282
 Nesvorný, D., Roig, F., and Ferraz-Mello, S.: 2000, *AJ* **119**, 953
 Petit, J., Kavelaars, J. J., Gladman, B., Jones, R. L., Parker, J. W., Van Laerhoven, C., Nicholson, P., Mars, G., Rousset, P., Mousis, O., Marsden, B., Bieryla, A., Murray, I., Ashby, M. L. N., Benavidez, P., Campo Bagatin, A., and Veillet, C.: 2011, *AJ* **142**, 131

- Schwamb, M. E., Brown, M. E., Rabinowitz, D. L., and Ragozzine, D.: 2010, *ApJ* **720**, 1691
- Thomas, F. and Morbidelli, A.: 1996, *Celestial Mechanics and Dynamical Astronomy* **64**, 209
- Tiscareno, M. S. and Malhotra, R.: 2009, *AJ* **138**, 827
- Tsiganis, K., Gomes, R., Morbidelli, A., and Levison, H. F.: 2005, *Nature* **435**, 459
- Wan, X. and Huang, T.: 2007, *MNRAS* **377**, 133
- Williams, J. G. and Benson, G. S.: 1971, *AJ* **76**, 167